

# Interplay between the symmetry energy and the strangeness content of neutron stars

Constança Providência<sup>1,\*</sup> and Aziz Rabhi<sup>1,2,†</sup>

<sup>1</sup>*Centro de Física Computacional, Department of Physics,  
University of Coimbra, 3004-516 Coimbra, Portugal*

<sup>2</sup>*Laboratoire de Physique de la Matière Condensée,  
Université de Tunis El-Manar, Campus Universitaire, Le Belvédère-1060, Tunisia*  
(Dated: August 22, 2018)

The effect of the density dependence of the nucleonic equation of state and the hyperon meson couplings on the star properties, including strangeness content, mass and radius, are studied within a relativistic mean field formalism. It is shown that there is still lacking information on the nucleonic equation of state at supra-saturation densities and on the hyperon interactions in nuclear matter that will allow a clear answer to the question whether the mass of the pulsar J1614-2230 could rule out exotic degrees of freedom from the interior of compact stars. We show that some star properties are affected in a similar way by the density dependence of the symmetry energy and the hyperon content of the star. To disentangle these two effects it is essential to have a good knowledge of the equation of state at supra-saturation densities. A linear correlation between the radius and the strangeness content of a star with a fixed mass is obtained.

PACS numbers: 21.65.-f 21.65.Ef 26.60.-c 97.60.Jd

## I. INTRODUCTION

The measurement of the mass of the mili-second pulsar PSR J1614-2230 with high precision,  $M = 1.97 \pm 0.04 M_\odot$  [1], has given origin to a large number of studies that discuss whether there is room for hyperons or other exotic degrees of freedom inside this star [2–7]. In particular microscopic calculations using the non-relativistic Brueckner-Hartree-Fock formalism predict a very large softening of the equation of state (EOS) when hyperons are taken into account, and are not even able to account for the standard neutron star masses of the order  $\sim 1.4 M_\odot$  [8]. The possibility that three-body-hyperonic forces could solve this problem was discussed in [2] by complementing the BHF calculation with a density dependent Skyrme like term based on the model [9] which mimics the many-body-term. Reasonable assumptions seem to exclude the appearance of stars with masses larger than  $1.6 M_\odot$ . It would be important to verify whether within a relativistic microscopic approach the same conclusions would be drawn. It is known that among the important effects included in the relativistic models, the saturation of the scalar field gives rise to effects that can be interpreted as many-body effects and could give rise to the extra repulsion needed [10].

Hyperons may appear in the inner core of neutron stars at densities of about  $2 - 3\rho_0$  and have first been introduced in relativistic mean-field nuclear models in [11–13]. In particular, in reference [13] the strange mesons  $\sigma^*$  and  $\phi$  have also been introduced. We will fix the couplings of the hyperons to mesons following a similar way to the one proposed in [13].

In [3] the authors have shown that it was essential to include the strange meson  $\phi$  in order to get stiff enough EOS that could describe a star with a mass of  $\sim 2M_\odot$ . The calculation was done within a relativistic mean-field (RMF) approach including only non-linear  $\sigma$ -meson terms. The authors have concluded that the compression modulus at saturation had little effect on the maximum mass, which, however, was very sensitive to the effective mass. Similar conclusions with respect to the EOS had been drawn in [14]. Within this approach a small effective mass at saturation requires a large sigma meson coupling that has to be compensated by a large nucleon-omega meson coupling, giving rise to large vector contributions at high densities, and, therefore, a stiff EOS and large star masses. If, however, constraints on the EOS like the ones coming from the flow analysis of nuclear matter in heavy ion collisions [15] are imposed, stiff EOS at high densities are ruled out. The softening of the EOS at large densities may be achieved including a quartic term on the  $\omega$ -meson as in [16] or density dependent couplings as in [17].

In the present study we will analyze how the content of strangeness of a star is defined by the properties of the nucleonic EOS and the hyperon-meson couplings. In particular we will discuss: a) the effect of the density dependence of the symmetry energy, b) the effect of the incompressibility of the EOS at 2-3 nuclear saturation density, c) the joint effect of these two properties together with the uncertainty on the hyperon couplings. The effect of the strange content on the maximum mass will be discussed. It will be shown not only that the presence of the strange mesons  $\sigma^*$  and  $\phi$  is important to give rise to a hard hyperonic EOS at large densities as already shown in [3, 5], but also that the density dependence of the EOS at 2-3 times saturation density has noticeable effects on the star properties. In [18], the authors study the implication of a soft EOS, as obtained from kaon production in heavy-ion collisions at these same densities [19], on the

\*Electronic address: cp@teor.fis.uc.pt

†Electronic address: rabhi@teor.fis.uc.pt

properties of compact star.

In order to be able to quantize the effects we take as reference the TM1 parametrization of relativistic mean-field nuclear models [16]. This model was fitted to the ground-state properties of several nuclei and to the Dirac-Brueckner-Hartree-Fock calculations at large densities. This last feature was only possible with the insertion of a quartic self-interaction  $\omega$  term which softens the vector meson field at high densities. The effect of this softening on the hyperon content will be discussed by varying the strength of the quartic term. The slope of the symmetry energy of TM1 at saturation  $L = 110$  MeV is too high according to the present experimental constraints coming from different nuclear properties, lying close to the upper limit of isospin diffusion in heavy ion collisions [20]. In order to test the effect of the symmetry energy slope we will introduce a non-linear  $\omega - \rho$  term as in [21] and change the coupling so that models with equivalent isoscalar properties of TM1 but different density dependence of the symmetry energy will be obtained. As discussed in [7, 21–23] this term reflects itself on the star properties, namely giving rise to a smaller radii. We will show that this effect is larger for nucleonic stars than for hyperonic stars and that, in fact, the presence of hyperons gives rise to a similar effect that masks the symmetry energy one.

In section II we present the formalism used, in section III the results are presented and discussed and finally in section IV some conclusions are drawn.

## II. FORMALISM

To describe the hadronic matter, we employ a relativistic mean-field (RMF) approach, in which the baryons interact via the exchange of mesons. The baryons considered in this work are nucleons ( $n$  and  $p$ ) and hyperons ( $\Lambda$ ,  $\Sigma$ , and  $\Xi$ ). The exchanged mesons include scalar and vector mesons ( $\sigma$  and  $\omega$ ), isovector meson ( $\rho$ ), and two additional hidden-strangeness mesons ( $\sigma^*$  and  $\phi$ ). The Lagrangian density includes several non-linear terms in order to describe adequately the saturation properties of nuclear matter. For neutron star matter consisting of neutral mixture of baryons and leptons in  $\beta$ -equilibrium, we start from the effective Lagrangian density of the non-linear Walecka model (NLWM) [16]

$$\begin{aligned} \mathcal{L}_{NLWM} = & \sum_B \bar{\Psi}_B [\gamma_\mu D_B^\mu - m_B^*] \Psi_B \\ & + \sum_l \bar{\psi}_l [i\gamma_\mu \partial^\mu - m_l] \psi_l \\ & + \frac{1}{2} (\partial_\mu \sigma \partial^\mu \sigma - m_\sigma^2 \sigma^2) - \frac{1}{3!} k \sigma^3 - \frac{1}{4!} \lambda \sigma^4 \\ & + \frac{1}{2} m_\omega^2 \omega_\mu \omega^\mu - \frac{1}{4} \Omega_{\mu\nu} \Omega^{\mu\nu} + \frac{1}{4!} \xi g_\omega^4 (\omega_\mu \omega^\mu)^2 \\ & + \frac{1}{2} m_\rho^2 \mathbf{b}_\mu \mathbf{b}^\mu - \frac{1}{4} \mathbf{B}_{\mu\nu} \mathbf{B}^{\mu\nu} \\ & + \Lambda_\omega (g_\omega^2 \omega_\mu \omega^\mu) (g_\rho^2 \mathbf{b}_\mu \cdot \mathbf{b}^\mu) \end{aligned}$$

$$\begin{aligned} & + \frac{1}{2} (\partial_\mu \sigma^* \partial^\mu \sigma^* - m_{\sigma^*}^2 \sigma^{*2}) \\ & + \frac{1}{2} m_\phi^2 \phi_\mu \phi^\mu - \frac{1}{4} \phi_{\mu\nu} \phi^{\mu\nu} \end{aligned} \quad (1)$$

where  $D_B^\mu = i\partial^\mu - g_{\omega B}\omega^\mu - g_{\phi B}\phi^\mu - g_{\rho B}\boldsymbol{\tau}_B \cdot \mathbf{b}^\mu$  and  $m_B^* = m_B - g_{\sigma B}\sigma - g_{\sigma^* B}\sigma^*$  is the baryon effective mass.  $\Psi_B$  and  $\psi_l$  are the baryon and lepton Dirac fields, respectively, and  $\sigma$ ,  $\omega$ , and  $\rho$  represent the scalar, vector, and vector-isovector meson fields, which describe the nuclear interaction. The coupling constants of mesons  $i = \sigma, \omega, \rho$  with baryon  $B$  are denoted by  $g_{iB}$  where the index  $B$  runs over the eight lightest baryons  $n, p, \Lambda, \Sigma^-, \Sigma^0, \Sigma^+, \Xi^-, \Xi^0$ , and the sum on  $l$  is over electrons and muons ( $e^-$  and  $\mu^-$ ). The baryon mass and the lepton mass are denoted by  $m_B$  and  $m_l$ , respectively. The constants  $k$  and  $\lambda$  are the weights of the scalar self-interaction terms and  $\boldsymbol{\tau}_B$  is the isospin operator. The mesonic field tensors are given by their usual expressions:  $\Omega_{\mu\nu} = \partial_\mu \omega_\nu - \partial_\nu \omega_\mu$ ,  $\mathbf{B}_{\mu\nu} = \partial_\mu \mathbf{b}_\nu - \partial_\nu \mathbf{b}_\mu$ , and  $\phi_{\mu\nu} = \partial_\mu \phi_\nu - \partial_\nu \phi_\mu$ .

In the RMF model, the meson fields are treated as classical fields, and the field operators are replaced by their expectation values. Applying the Euler-Lagrange equations to Eq.(1) and using the mean-field approximation, we obtain the following meson field equations of motion as following, with  $g_{iB} = x_{iB} g_i$ ,

$$\sigma_0 = \frac{g_\sigma}{m_{\sigma,eff}^2} \sum_B \frac{x_{\sigma B}}{\pi^2} \int_0^{k_F^B} \frac{m_B^* k^2 dk}{\sqrt{k^2 + m_B^{*2}}} \quad (2)$$

$$\omega_0 = \frac{g_\omega}{m_{\omega,eff}^2} \sum_B \frac{x_{\omega B} (k_F^B)^3}{3\pi^2}, \quad (3)$$

$$b_0 = \frac{g_\rho}{m_{\rho,eff}^2} \sum_B \frac{x_{\rho B} \tau_{3B} (k_F^B)^3}{3\pi^2}, \quad (4)$$

$$\sigma_0^* = \frac{g_{\sigma^*}}{m_{\sigma^*}^2} \sum_B \frac{x_{\sigma^* B}}{\pi^2} \int_0^{k_F^B} \frac{m_B^* k^2 dk}{\sqrt{k^2 + m_B^{*2}}} \quad (5)$$

$$\phi_0 = \frac{g_\phi}{m_\phi^2} \sum_B \frac{x_{\phi B} (k_F^B)^3}{3\pi^2}, \quad (6)$$

where

$$m_{\sigma,eff}^2 = m_\sigma^2 + \frac{k}{2} \sigma_0 + \frac{\lambda}{6} \sigma_0^2 \quad (7)$$

$$m_{\omega,eff}^2 = m_\omega^2 + \frac{\xi}{6} g_\omega^4 \omega_0^2 + 2\Lambda_\omega g_\omega^2 g_\rho^2 b_0^2, \quad (8)$$

$$m_{\rho,eff}^2 = m_\rho^2 + 2\Lambda_\omega g_\omega^2 g_\rho^2 \omega_0^2. \quad (9)$$

We see that the non-linear  $\omega$  and  $\rho$  terms give rise to effective masses for the  $\omega$  and  $\rho$  mesons that increase with density, giving rise to a softening of the vector fields at large densities. In this work, we employ the TM1 parameter set of the RMF model. The meson-hyperon and the strange meson-hyperon coupling constants  $g_{\omega H}$ ,  $g_{\rho H}$ ,  $g_{\sigma^* H}$ , and  $g_{\phi H}$  are determined by using SU(6) symmetry

$$\frac{1}{3} g_{\omega N} = \frac{1}{2} g_{\omega \Lambda} = \frac{1}{2} g_{\omega \Sigma} = g_{\omega \Xi},$$

TABLE I: Coupling constants and masses for the TM1 and TM1-2 models which have the same saturation properties: saturation density  $\rho_0 = 0.145 \text{ fm}^{-3}$ , binding energy  $E/A = -16.30 \text{ MeV}$ , symmetry energy  $J = 36.93 \text{ MeV}$ , incompressibility  $K = 281.28 \text{ MeV}$ , effective mass  $M^*/M = 0.63$ .

Model	$\left(\frac{g_\sigma}{m_\sigma}\right)^2$ (fm) <sup>2</sup>	$\left(\frac{g_\omega}{m_\omega}\right)^2$ (fm) <sup>2</sup>	$\left(\frac{g_\rho}{m_\rho}\right)^2$ (fm) <sup>2</sup>	$k/M$	$\lambda$	$\xi$
TM1	15.0125	10.1187	5.6434	3.0655	2.7333	0.06
TM1-2	14.9065	9.9356	5.6434	3.5351	-47.8812	0.04

$$g_{\rho N} = g_{\rho \Lambda} = \frac{1}{2}g_{\rho \Sigma} = g_{\rho \Xi}$$

$$2g_{\phi \Lambda} = 2g_{\phi \Sigma} = g_{\phi \Xi} = -\frac{2\sqrt{2}}{3}g_{\omega N} \quad (10)$$

where  $N$  means nucleon ( $g_{iN} \equiv g_i$ ). The scalar coupling constants are chosen to give reasonable potentials. The coupling constants  $g_{\sigma H}$  of the hyperons with the scalar meson  $\sigma$  are adjusted to the potential depths  $U_H^{(N)}$  felt by a hyperon  $H$  in symmetric nuclear matter at saturation following the relation

$$U_H^N = x_{\omega H}V_\omega - x_{\sigma H}V_\sigma \quad (11)$$

with  $x_{i,H} = g_{i,H}/g_i$ ,  $V_\omega \equiv g_\omega \omega_0$  and  $V_\sigma \equiv g_\sigma \sigma_0$  are the nuclear potentials for symmetric nuclear matter at saturation density. For the present work we will fix  $U_\Lambda^N = -28 \text{ MeV}$ , and use  $U_\Sigma^N = -30, 0, 30 \text{ MeV}$ , and for  $U_\Xi^N$  we will use different values  $-18, 0$ , and  $18 \text{ MeV}$ . For the  $\sigma^*$  meson we consider a weak  $YY$  coupling and take  $U_\Lambda^\Lambda \sim -5 \text{ MeV}$ , together with  $2g_{\sigma^* \Lambda} = 2g_{\sigma^* \Sigma} = g_{\sigma^* \Xi}$ . All hyperon coupling ratios  $\{g_{\sigma H}, g_{\omega H}, g_{\rho H}\}_{H=\Lambda, \Sigma, \Xi}$  are determined once the coupling constants  $\{g_\sigma, g_\omega, g_\rho\}$  of the nucleon sector are given. The hyperons masses are taken to be  $m_\Lambda = 1116 \text{ MeV}$ ,  $m_{\Sigma^+} = 1189 \text{ MeV}$ ,  $m_{\Sigma^0} = 1193 \text{ MeV}$ ,  $m_{\Sigma^-} = 1197 \text{ MeV}$  and  $m_{\Xi^0} = 1315 \text{ MeV}$ ,  $m_{\Xi^-} = 1321 \text{ MeV}$ , while the strange meson masses are  $m_{\sigma^*} = 980 \text{ MeV}$  and  $m_\phi = 1020 \text{ MeV}$ .

For neutron star matter consisting of a neutral mixture of baryons and leptons, the  $\beta$  equilibrium condition without neutrino trapping are given by

$$\begin{aligned} \mu_p &= \mu_{\Sigma^+} = \mu_n - \mu_e \\ \mu_\Lambda &= \mu_{\Sigma^0} = \mu_{\Xi^0} = \mu_n \\ \mu_{\Sigma^-} &= \mu_{\Xi^-} = \mu_n + \mu_e \\ \mu_\mu &= \mu_e \end{aligned} \quad (12)$$

where  $\mu_i$  is the chemical potential of species  $i$ . The chemical potentials of baryons and leptons are given by

$$\begin{aligned} \mu_B &= \sqrt{k_F^{B^2} + m_B^{*2}} + g_{\omega B}\omega_0 + g_{\rho B}\tau_{3B}b_0 + g_{\phi B}\phi_0 \\ \mu_l &= \sqrt{k_F^{l^2} + m_l^2}. \end{aligned} \quad (13)$$

and the charge neutrality condition is written by

$$\rho_p + \rho_{\Sigma^+} = \rho_e + \rho_\mu + \rho_{\Sigma^-} + \rho_{\Xi^-}, \quad (14)$$

where  $\rho_i = (k_F^i)^3 / (3\pi^2)$  is the number density of species  $i$ . We solve the coupled equations self-consistently at a given baryon density  $\rho_B = \rho_n + \rho_p + \rho_\Lambda + \rho_{\Sigma^+} + \rho_{\Sigma^0} + \rho_{\Sigma^-} + \rho_{\Xi^0} + \rho_{\Xi^-}$ . Through the energy-momentum tensor, we obtain the total energy density and the pressure of the neutron star matter

$$\begin{aligned} \varepsilon &= \sum_B \frac{1}{\pi^2} \int_0^{k_F^B} \sqrt{k^2 + m_B^{*2}} k^2 dk \\ &+ \sum_{l=e, \mu} \frac{1}{\pi^2} \int_0^{k_F^l} \sqrt{k^2 + m_l^2} k^2 dk \\ &+ \frac{1}{2}m_\sigma^2 \sigma_0^2 + \frac{k}{6}\sigma_0^3 + \frac{\lambda}{24}\sigma_0^4 + \frac{1}{2}m_\omega^2 \omega_0^2 + \frac{1}{8}\xi g_\omega^4 \omega_0^4 \\ &+ \frac{1}{2}m_\rho^2 b_0^2 + 3\Lambda_\omega g_\omega^2 g_\rho^2 \omega_0^2 b_0^2 \\ &+ \frac{1}{2}m_{\sigma^*}^2 \sigma^{*2} + \frac{1}{2}m_\phi^2 \phi_0^2, \end{aligned} \quad (15)$$

$$\begin{aligned} P &= \sum_B \frac{1}{3\pi^2} \int_0^{k_F^B} \sqrt{k^2 + m_B^{*2}} k^2 dk \\ &+ \sum_{l=e, \mu} \frac{1}{3\pi^2} \int_0^{k_F^l} \sqrt{k^2 + m_l^2} k^2 dk \\ &- \frac{1}{2}m_\sigma^2 \sigma_0^2 - \frac{k}{6}\sigma_0^3 - \frac{\lambda}{24}\sigma_0^4 + \frac{1}{2}m_\omega^2 \omega_0^2 + \frac{1}{24}\xi g_\omega^4 \omega_0^4 \\ &+ \frac{1}{2}m_\rho^2 b_0^2 + \Lambda_\omega g_\omega^2 g_\rho^2 \omega_0^2 b_0^2 \\ &- \frac{1}{2}m_{\sigma^*}^2 \sigma^{*2} + \frac{1}{2}m_\phi^2 \phi_0^2. \end{aligned} \quad (16)$$

### III. RESULTS AND DISCUSSIONS

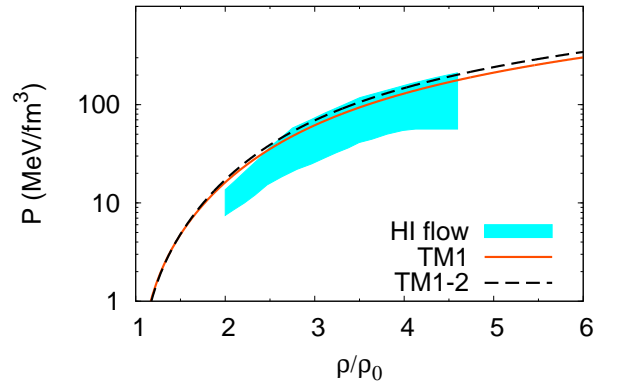


FIG. 1: (Color online) EOS for TM1, TM1-2 and FSU [24] above saturation density. The shaded region represents constraints imposed by heavy ion flow [15].

In order to better understand the effect of the symmetry energy and the incompressibility of the EOS at high densities together with the uncertainty on the hyperon

interaction on the strangeness content, the mass and radius of the stars, we consider the parametrization TM1, a parametrization that satisfies the heavy-ion flow constraints for symmetric matter at  $2-3\rho_0$  [15], see Fig. 1. Even though in the following we will use parametrizations which satisfy this constraint, it is important to point out that, since it is hard to model flow in transport simulations, this constraint should be taken with care.

We will also consider two variations of TM1: a) we will consider the EOS of TM1 with a smaller quartic omega term, but with the same properties at saturation. We designate this parametrization as TM1-2, and, as shown in Fig. 1, it is stiffer than with TM1 at supra-saturation densities but still within the constraints imposed by heavy ion flow [15]; b) the symmetry energy slope of TM1 at saturation density is  $L = 110$  MeV, a value which is presently considered too high (see [20, 25]), and, therefore, we also take a second parametrization changing the isovector channel of TM1 by including a non-linear  $\omega\rho$  term that makes the symmetry energy slope softer at supra-saturation densities. We will choose  $L = 55, 70$  and  $80$  MeV. Using these nucleonic EoS we will test different hyperon interactions in nuclear matter.

For the hyperon potentials in symmetric nuclear matter at saturation we take  $U_\Lambda^N = -28$  MeV,  $U_\Sigma^N = 30$  MeV and  $U_\Xi^N = \pm 18$  MeV. The two values of  $U_\Xi^N$  take into account some uncertainty on the experimental data on this potential [26]. Finally, we also consider the inclusion of the strange mesons  $\sigma^*, \phi$ . According to recent experimental  $\Lambda - \Lambda$ -hypernuclear data, the  $\Lambda - \Lambda$  interaction is only weakly attractive [27]. The effect of the small attractiveness of the hyperon-hyperon coupling will be considered by choosing a) a weak  $g_{\sigma^*H}$  coupling; b) the extreme value  $g_{\sigma^*H} = 0$ .

In Fig. 2, top panel, the EOS for the different choices of the nucleonic and hyperonic parametrizations are shown. The full dots indicate the central density of the most massive stable stars within each parametrization. We do not include the EOS without hyperons in the figure in order not to burden it, but, as shown in Fig. 7 of [28] it corresponds to the hardest EOS and gives rise to a maximum star mass of  $2.18M_\odot$  for  $L = 110$  MeV and  $2.13M_\odot$  if  $L = 55$  MeV (see Table II). The full lines describe the EOS without the strange mesons and these are the softer EOS. In this case the difference between the  $L = 55$  MeV (thick lines) and  $L = 110$  MeV (thin lines) is the largest. This is also the situation when the  $\Xi$  potential has the largest effect. The strangeness content corresponding to these EOS, see bottom panel of Fig. 2, explains the differences: the onset of strangeness occurs at lower densities for  $L = 110$  MeV and increases faster. A more attractive  $\Xi$  potential also gives rise to larger strangeness fractions. An interesting effect is that although having a softer EOS, stars whose strangeness fraction increase faster with density have lower central densities, as if the star did not support more than a given strangeness content.

As already discussed in [7, 22], a smaller slope  $L$  im-

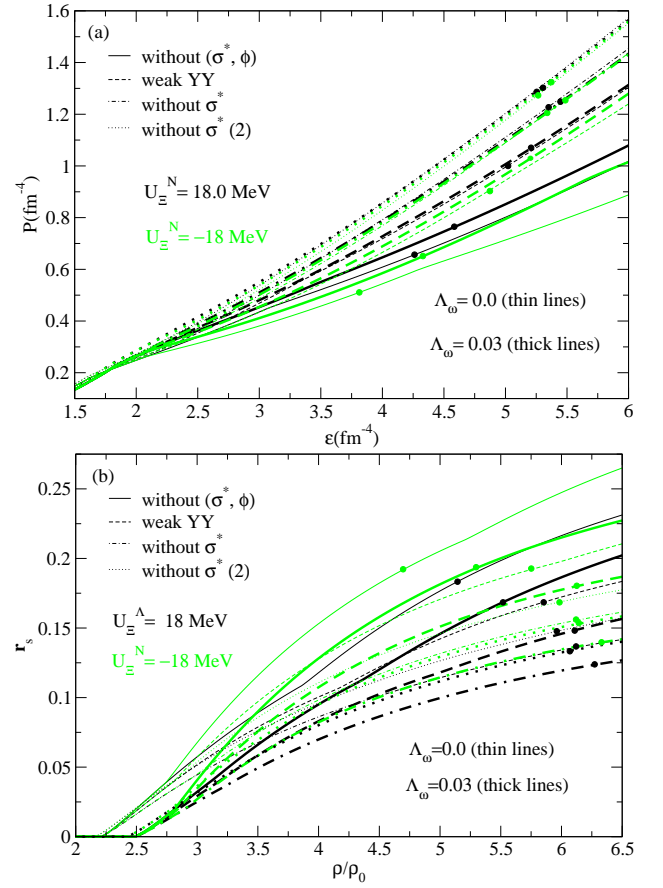


FIG. 2: (Color online) Pressure versus energy density (top) and strangeness fraction versus baryonic density (bottom) for TM1 model, for different values of  $U_\Xi^N$  ( $-18$  MeV green curves and  $+18$  MeV black curves) and the  $\Lambda_\omega$  coupling (0 corresponding to  $L = 110$  MeV thin curves and  $0.03$  for  $L = 55$  MeV thick lines). The dots identify the maximum mass configuration. The dotted curves correspond to smaller quartic omega term.

plies a softer increase of the strangeness fraction with density. However, because the central density of these stars is larger, it is important to study the total hyperon content of the star. This will be done by calculating for each star the total strangeness number

$$N_S = 4\pi \int_0^R \frac{\rho_s r^2}{\sqrt{1 - 2m(r)/r}} dr,$$

where  $m(r)$  is the mass inside the radius  $r$ .

Including strange mesons washes out the effect of the symmetry energy and of the  $\Xi$  optical potential on the EOS, mainly if only the  $\phi$  meson, that gives rise to extra repulsion between hyperons, is included (dash-dotted lines).

Taking the nucleonic TM1-2 EOS, a stiffer EOS than TM1 at large densities (dotted lines) the EOS remains always stiffer than TM1 although having a larger strangeness content.



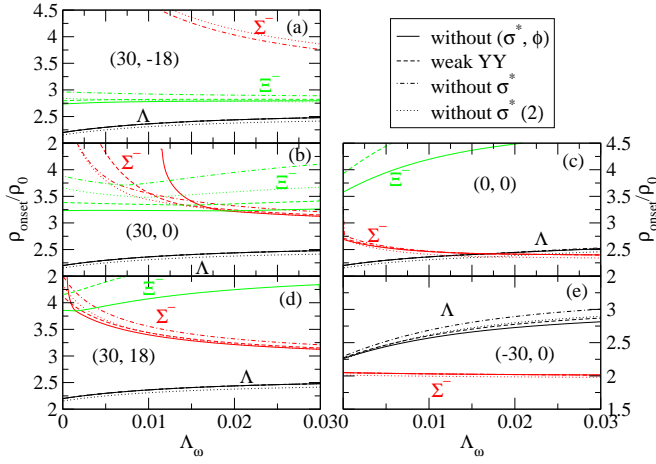


FIG. 3: (Color online) Onset of the  $\Lambda$ , the  $\Sigma^-$ , and the  $\Xi^-$  hyperons as a function of the parameter  $\Lambda_\omega$  and with  $U_\Lambda^N = -28$  and several values of  $U_\Sigma^N$  and  $U_\Xi^N$  in symmetric nuclear matter at saturation. The limiting values of  $\Lambda_\omega$  correspond to 110 MeV (0) and 55 MeV (0.03). The pair of values given in each graph refers to  $(U_\Sigma^N, U_\Xi^N)$ .

We have seen that the symmetry energy affects the onset of hyperons, namely postponing to larger densities the onset of hyperons for smaller  $L$  values. In Fig. 3 it is shown that the different hyperons are affected in a different way by the symmetry energy. In this figure we plot as a function of the coupling  $\Lambda_\omega$ ,  $\Lambda_\omega = 0$  (0.03) corresponds to 110 (55) MeV, the onset of the  $\Lambda$ ,  $\Sigma^-$  and  $\Xi^-$ . It is seen that the onset of  $\Sigma^-$  always decreases with the decrease of  $L$ , due to its larger isospin. On the other hand, the onset of  $\Lambda$  occurs at larger densities. The  $\Xi^-$  never is the first hyperon to appear due to its large mass, but, according to the attractiveness of its potential in nuclear matter, it can appear as the second hyperon. If the repulsiveness of the  $\Sigma^-$  in nuclear matter is confirmed we may expect that the  $\Lambda$  is the first hyperon to set on and, therefore, with a smaller slope  $L$  the onset of strangeness occurs at larger densities. However, if the optical potential of the  $\Sigma^-$  in nuclear matter is only slightly repulsive there may be a competition between the onset of  $\Lambda$  and  $\Sigma^-$  depending on the  $L$ , with smaller values of  $L$  favoring the  $\Sigma^-$  hyperon (see top figure of the right column).

Lepton fractions are also strongly affected by the symmetry energy density dependence and the hyperon interaction. From the equations of motion for the mesons, Eqs. (6) and (9), it is seen that the non-linear  $\omega - \rho$  term gives rise to an effective mass for the  $\rho$ -meson that increases with density, giving rise to a weaker  $\rho$ -meson field, Eq. (6). An immediate consequence is a smaller asymmetry proton-neutron term in the total energy and larger allowed differences between neutrons and protons. Smaller proton fractions give rise to smaller electron fractions for smaller slopes  $L$ , as is clearly seen in Fig. 4. Including hyperons will further reduce the electron fraction mainly if the hyperon couplings favor the appearance of negatively charged hyperons. This explains the difference

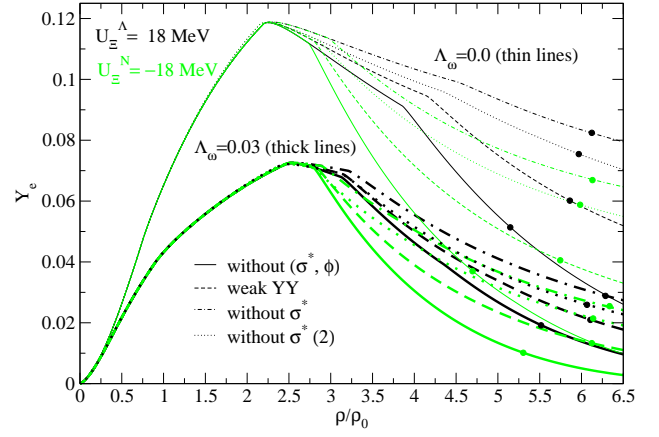


FIG. 4: (Color online) Electrons fraction  $Y_e = \rho_e/\rho_0$  as function of the ratio  $\rho/\rho_0$  for TM1 model and different values of  $U_\Xi^N$  and the  $\Lambda_\omega$  coupling (see caption of Fig. 2). The dots identify the maximum mass configuration.

between the green curves with  $U_\Xi^N = -18$  MeV which favors the onset of  $\Xi^-$ , with respect to the black curves. The onset of neutrally charged hyperons also reduces the electron fraction although not so strongly. For  $L = 110$  MeV the electron fraction at the center of the star can go from 0.04 to 0.1 depending on the hyperon interaction. This uncertainty reduces to a fraction between 0.01 and 0.03 for  $L = 55$  MeV. Smaller electron fractions are generally connected to larger neutrino fractions in matter with trapped neutrinos and therefore, the cooling in the early seconds of a proton-neutron star will be strongly affected by the slope  $L$ .

By solving the Tolman-Oppenheimer-Volkoff equations [29], resulting from Einstein's general relativity equations for spherically symmetric and static stars, the neutron star profiles are obtained from the EOS studied, for several values of  $U_\Xi^N$  and the  $\Lambda_\omega$  coupling. For the outer crust EOS and the bottom inner crust EOS we consider the BPS EOS [30].

We now analyze the gravitational mass/radius curves of the families of stars described by the above EOS and their strangeness content (Fig. 5 and Table II). In the bottom panel of the Fig. 5 we plot, as a function of the gravitational mass, the total strangeness number of the star over the total baryonic number, which measures the total strangeness content of the star. The strangeness degree of freedom is only present in stars with gravitational masses above  $1.5 M_\odot$ , and the strangeness content generally attains larger values for  $L = 110$  MeV (thin lines).

In order to help the analysis of this information, in Fig. 6 we plot the radius of a star with a mass  $1.67 M_\odot$  similar to the mass of the pulsar PSR J1903+0327 ( $1.67 \pm 0.02 M_\odot$ ) [31] as a function of its strangeness content. The largest strangeness fractions were obtained considering an attractive potential for the  $\Sigma^-$  meson. It is interesting to notice that two almost parallel straight lines are obtained: for  $L = 110$  MeV the slope is -11.27

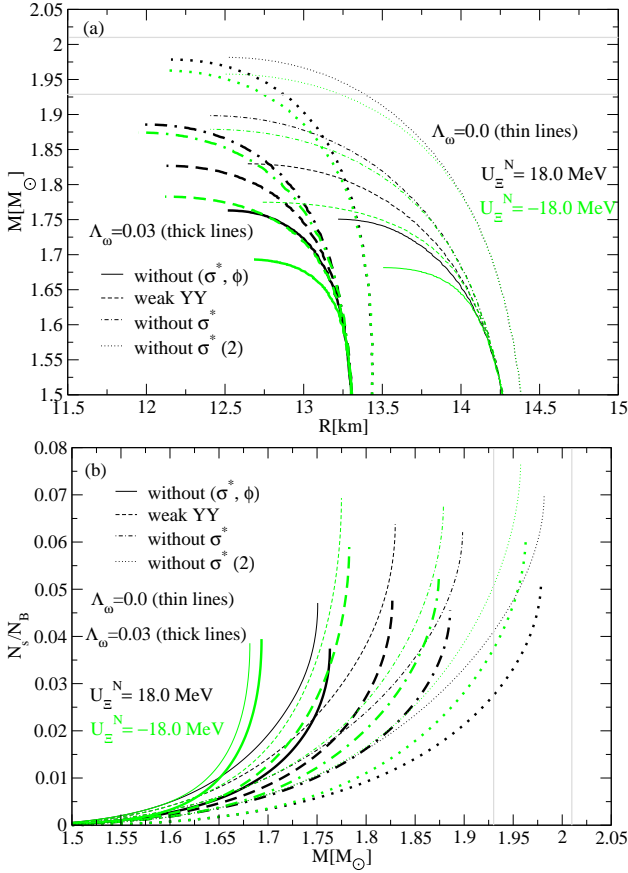


FIG. 5: (Color online) Gravitational mass versus the radius (top panel) and strangeness number over the total baryonic number versus gravitational mass (bottom panel) for TM1, and different values of  $U_\Xi^N$  and the  $\Lambda_\omega$  coupling. The lines indicate the lower and upper limit of the PSR J1614-2230 mass.

$\pm 4\%$  km and for  $L = 55$  MeV the slope is  $-10.62 \pm 1\%$  km. The straight lines cross the vertical axis for a nucleonic star with no hyperons. The slope is almost independent of  $L$ .

The information related to the maximum mass configurations presented in Table II is partially plotted in Fig. 7 for the parametrization TM1. We have considered four values of  $\Lambda_\omega$  corresponding to  $L = 55, 70, 80$  and  $110$  MeV in order to be able to discuss the effect of the symmetry energy slope.

Some general conclusions may be drawn with respect to the strangeness content: a) if the strange mesons are not included, we get the smallest masses [see Table II and red ( $U_\Xi^N = -18$  MeV), green ( $U_\Xi^N = +18$  MeV) symbols in Fig. 7a)]. A faster increase of the strangeness content seems to be the reason for this behavior. These are also the stars with the smallest strangeness content [see Fig. 7d)]; b) the maximum star mass changes with  $L$ , and stars with an intermediate  $L$  have the smallest masses and, generally, have the largest central densities [see Fig. 7a) and e)]. There are two competing factors

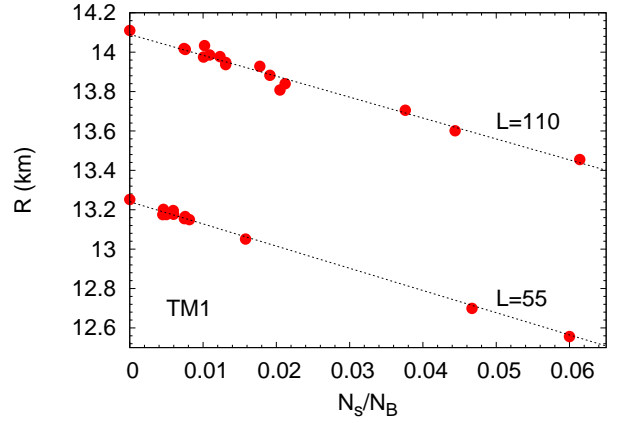


FIG. 6: (Color online) Radius of a star with mass  $1.67 M_\odot$  as a function of the strangeness content, for TM1 with  $L = 110$  MeV (top line with slope  $-11.27 \pm 4\%$  km) and TM1 with  $\omega\rho$  term and  $L = 55$  MeV (bottom line with slope  $-10.62 \pm 1\%$  km).

that define this behavior: on one hand a larger  $L$  corresponds to a harder EOS because the symmetry energy increases faster with the density, on the other hand a larger  $L$  favors larger strangeness fractions which softens the EOS. The first one gives rise to smaller central densities and larger radii, while the second one leads to the opposite; c) the strangeness content depends on the hyperon interaction, and, in particular, on the  $\Xi$  potential in the present study. If  $U_\Xi^N = +18$  MeV (triangles) the masses are larger and the strangeness fractions generally smaller; d) including the strange mesons gives rise to more massive stars which may have larger strangeness contents. In this case the strangeness content is always smaller for a smaller slope  $L$ , and its maximum value is of the order 0.04-0.05 according to the hyperon interaction if  $L = 55$  MeV. The upper limit can go to 0.07-0.08 if  $L = 110$  MeV, Fig. 7d). Larger fractions may be obtained if the  $U_\Sigma^N$  is considered attractive.

As discussed before, comparing stars with the same mass the strangeness content depends on the hyperon-meson interaction, and, for instance, a  $1.67 M_\odot$  may have a strangeness fraction that goes from 0.005 to 0.115. The largest strangeness fraction was obtained with  $U_\Sigma^N = -30$  MeV, no strange mesons and  $L = 55$  MeV. For  $L = 110$  MeV there is no stable star with this mass for these couplings.

We conclude that both the symmetry energy and the strangeness content may give rise to similar effects on some properties of the stars such as the radius. These two effects may be partially disentangled by analyzing stars in different mass ranges, since hyperons only exist in massive enough stars, in the present case only if  $M > 1.5 M_\odot$ . On the other hand low mass stars do not test the EOS at large densities. For TM1 the central density of a star with  $M = 1.2 M_\odot$  is of the order of  $2\rho_0$ . The effect on the radius of a star with a mass  $M = 1.67 M_\odot$

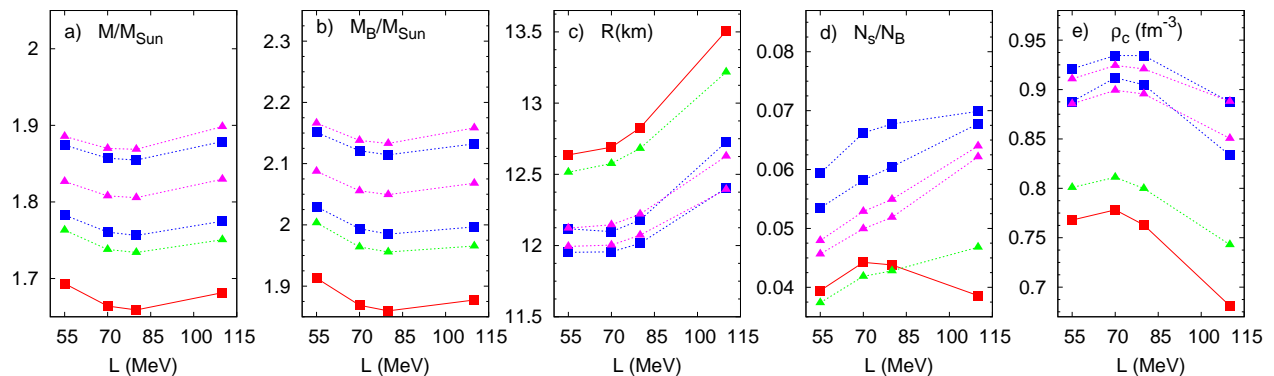


FIG. 7: (Color online) Properties of maximum mass stars obtained with  $L = 55, 70, 80$  and  $110$  MeV, for TM1:  $U_{\Xi}^N = +18$  MeV (triangles) without (green) and with (pink)  $YY$  interaction;  $U_{\Xi}^N = -18$  MeV (squares) without (red) and with (blue)  $YY$  interaction: gravitational mass, baryonic mass, star radius, strangeness content and central density.

is similar if the slope  $L$  decreases from  $110$  MeV to  $55$  MeV or the total strangeness fraction in the star increases from zero to  $10\%$ . In both cases the star radius suffers a decrease of  $1$  km.

In [22, 28] it was shown that a smaller  $L$  makes the nucleonic EOS softer giving rise to less massive stars with smaller radius that varies approximately linearly with  $L$ . The inclusion of hyperons softens the EOS but if the strange mesons are included although the strangeness fraction as a function of density is smaller, the total strangeness content in the star will be larger than when only non-strange mesons are included. If hyperonic degrees of freedom are included the radius of the star decreases. An extra decrease of the radius occurs when a smaller  $L$  is considered, however, this effect is not so strong as in nucleonic stars.

An attractive or repulsive optical potential of the hyperons, in the present study  $U_{\Xi}^N$ , clearly affects the fraction of strangeness as a function of density. A large fraction of strangeness at smaller densities makes the EOS too soft and smaller maximum masses and central densities are obtained. This effect almost disappears if strange mesons are included.

At a given density the fraction of strangeness is smaller for a softer symmetry energy. As a result, although the initial nucleonic EOS is softer, a smaller hyperon fraction may give rise to a slightly larger maximum mass, *e.g.*  $1.76 M_{\odot}$  for  $L=55$  MeV instead of  $1.75 M_{\odot}$  for  $L=110$  MeV if  $U_{\Xi}^N = 18$  MeV or  $1.69 M_{\odot}$  for  $L=55$  MeV instead of  $1.68 M_{\odot}$  for  $L=110$  MeV if  $U_{\Xi}^N = -18$  MeV. This effect was also observed in the calculation with the QMC model [7]. This is not anymore true when the strange mesons are included because it brings extra repulsion to the EOS. Therefore, an EOS with a larger strangeness content may become harder.

In this schematic study the largest mass obtained for hyperonic stars is  $1.96 M_{\odot}$ , compatible with the mass of the pulsar PSR J1614-2230,  $1.97 \pm 0.04 M_{\odot}$ . However, there are still many uncertainties on the hyperon interaction in nuclear matter and the EOS of nucleonic matter

at supra-saturation densities. It is, therefore, not possible to take firm conclusions with respect to the possible existence of hyperons inside compact stars, except that it seems important to include extra repulsion between hyperons at high densities through the inclusion of strange mesons, as was proposed in [3].

#### IV. CONCLUSION

The density dependence of the EOS and the hyperon couplings have both a strong effect on the mass and radius of the star. We have tested different hyperon-meson parametrizations, using information from hyper-nuclei to fix the couplings, and different nucleonic properties at supra-saturation density within the limits of experimental constraints, namely the density dependence of the symmetry energy and the incompressibility at large densities.

The chosen nucleonic EOS cover different density dependences of both the isoscalar and isovector channels of the EOS. We have used an EOS with a quite high incompressibility at saturation,  $K = 281$  MeV. However, the non-linear vector meson quartic term softens the EOS at supra-saturation densities in such a way that the results from Dirac-Brueckner-Hartree-Fock calculations are reproduced [16], and the constraints imposed by heavy ion collisions [15] are satisfied. Also the slope of the symmetry energy of this model at saturation is probably too high according to present experimental information. Therefore, we have tested other EOS, with a softer symmetry energy and with a harder EOS at supra-saturation densities but still within the constraints of [15]. A softer EOS at saturation or above saturation will not favor so much the onset of hyperons, therefore, smaller hyperon contents and larger hyperon onset densities are expected. However, we should point out that a softer EOS at saturation or just above will allow that larger central densities are attained in the star, and, therefore, it is expected that the exotic degrees like hyperons will be present in

TABLE II: Properties of maximum mass stars obtained with the TM1 [16], TM1-2 and FSU [24] nucleonic EOS and with the corresponding hyperonic EOS with  $U_{\Lambda}^N = -28$  MeV and  $U_{\Sigma}^N = 30$  MeV and different values of  $U_{\Xi}^N$ .

	$\Lambda_{\omega}$	$M_G[M_{\odot}]$	$M_b[M_{\odot}]$	$R[\text{km}]$	$E_c(\text{fm}^{-4})$	$\frac{N_s}{\rho_B}$	$\rho_c(\text{fm}^{-3})$
no hyperons, TM1	0.0	2.18	2.54	12.39	5.36	-	0.85
	0.03	2.13	2.51	11.92	5.61	-	0.90
no hyperons, TM1-2	0.0	2.29	2.69	12.57	5.15	-	0.81
	0.03	2.25	2.66	12.14	5.37	-	0.86
no hyperons, FSU	0.03	1.72	1.97	10.85	7.07	-	1.15
$U_{\Xi}^N = -18$ MeV							
Without $(\sigma^*, \phi)$ , TM1	0.0	1.68	1.88	13.51	3.81	0.0386	0.68
	0.03	1.69	1.91	12.64	4.33	0.0395	0.77
Without $(\sigma^*, \phi)$ , TM1-2	0.0	1.74	1.95	13.52	3.86	0.0479	0.68
	0.03	1.77	2.01	12.70	4.34	0.0486	0.76
Without $\sigma^*$ , TM1	0.0	1.88	2.13	12.40	5.34	0.0678	0.89
	0.03	1.87	2.15	11.95	5.51	0.0535	0.92
Without $\sigma^*$ , TM1-2	0.0	1.96	2.23	12.50	5.26	0.0773	0.87
	0.03	1.96	2.27	12.10	5.37	0.0617	0.89
With $(\sigma^*, \phi)$ , weak YY, TM1	0.0	1.77	2.00	12.72	4.87	0.0699	0.83
	0.03	1.78	2.03	12.12	5.19	0.0594	0.89
With $(\sigma^*, \phi)$ , weak YY, TM1-2	0.0	1.84	2.08	12.76	4.90	0.0818	0.83
	0.03	1.86	2.13	12.21	5.14	0.0694	0.87
$U_{\Xi}^N = 0.0$ MeV							
Without $(\sigma^*, \phi)$ , TM1	0.0	1.72	1.93	13.38	4.02	0.0412	0.71
	0.03	1.74	1.97	12.62	4.39	0.0350	0.77
Without $(\sigma^*, \phi)$ , TM1-2	0.0	1.79	2.01	13.44	4.00	0.0484	0.70
	0.03	1.82	2.07	12.75	4.33	0.0417	0.76
Without $\sigma^*$ , TM1	0.0	1.89	2.15	12.42	5.33	0.0628	0.88
	0.03	1.89	2.17	12.00	5.44	0.0460	0.91
Without $\sigma^*$ , TM1-2	0.0	1.98	2.26	12.53	5.23	0.0712	0.86
	0.03	1.98	2.29	12.16	5.28	0.0526	0.88
With $(\sigma^*, \phi)$ , weak YY, TM1	0.0	1.81	2.04	12.73	4.88	0.0636	0.83
	0.03	1.81	2.07	12.19	5.10	0.0488	0.87
With $(\sigma^*, \phi)$ , weak YY, TM1-2	0.0	1.88	2.13	12.81	4.84	0.0730	0.82
	0.03	1.90	2.18	12.33	5.00	0.0568	0.85
$U_{\Xi}^N = 18$ MeV							
Without $(\sigma^*, \phi)$ , TM1	0.0	1.75	1.97	13.22	4.24	0.0468	0.74
	0.03	1.76	2.00	12.51	4.58	0.0374	0.80
Without $(\sigma^*, \phi)$ , TM1-2	0.0	1.82	2.05	13.28	4.23	0.0542	0.74
	0.03	1.84	2.11	12.65	4.51	0.0433	0.78
Without $\sigma^*$ , TM1	0.0	1.90	2.16	12.39	5.36	0.0622	0.89
	0.03	1.89	2.17	11.99	5.44	0.0456	0.91
Without $\sigma^*$ , TM1-2	0.0	1.98	2.27	12.50	5.26	0.0701	0.87
	0.03	1.98	2.29	12.15	5.29	0.0519	0.88
Without $\sigma^*$ , FSU	0.03	1.53	1.71	10.94	6.87	0.0348	1.16
With $(\sigma^*, \phi)$ , weak YY, TM1	0.0	1.83	2.07	12.63	5.03	0.0640	0.85
	0.03	1.83	2.09	12.12	5.21	0.0479	0.89
With $(\sigma^*, \phi)$ , weak YY, TM1-2	0.0	1.91	2.17	12.71	4.97	0.0728	0.83
	0.03	1.91	2.20	12.27	5.09	0.0548	0.86

less massive stars.

The present study estimates an upper limit of the expected hyperon content within RMF models taking into account the existing experimental constraints from heavy-ion collisions [15].

The effect of the density dependence of the symmetry energy on low mass neutron stars,  $M < 1.4M_{\odot}$ , with

no hyperon content, has been discussed within the RMF formalism in [23]. In the present study, we focus on hyperonic stars. For the nucleonic EOS used, the hyperon degrees of freedom are present only for densities above 2.2 to 2.5  $\rho_0$ , and inside stars with a mass larger than 1.5  $M_{\odot}$ . However, using a softer EOS like FSU [24], hyperonic stars have a mass above 1.2  $M_{\odot}$ . Since the EOS is



softer, matter is more easily compressed and exotic degrees of freedom occur in less massive stars. In this case, the strangeness content in the most favorable conditions discussed in the present paper does not exceed 0.035 of the total baryonic number in a maximum mass configuration with  $M = 1.52 M_{\odot}$ .

We conclude that a softer symmetry energy gives rise to smaller stars with smaller strangeness content. The maximum gravitational and baryonic mass and the central densities depend on the slope  $L$  on a non linear way, and intermediate  $L$  values may give smaller masses and larger central densities. It was also shown that for a star with a fixed mass the radius of the star decreases linearly with the increase of the total strangeness content. In particular a 1km decrease of the radius of a  $1.67 M_{\odot}$  star may be explained if the slope of the symmetry energy decreases from 110 to 55 MeV or the strangeness to baryon fraction increases from zero to  $\sim 0.09$ .

It was also shown that a softer symmetry energy corresponds to a slower increase of the hyperon fraction with density [7, 22]. However, the onset of strangeness depends on the charge of the hyperons. Negatively charged hyperons set on at smaller densities while neutral hyperons appear at larger densities for smaller values of  $L$ . If it is confirmed that the potential of  $\Sigma^-$  is repulsive in symmetric nuclear matter at saturation we may expect that  $\Lambda$  is the hyperon that arises at lower densities, and, in this case, the onset of strangeness occurs at larger densities with smaller slope  $L$ .

For a nucleonic EOS we would expect that the softer the EOS is, the larger are the central densities attained and the smaller the radius. However, hyperons will affect this simple relation and we have obtained larger central densities with harder EOS when no exchange of strange mesons or just a weakly attractive hyperon-hyperon interaction are considered. This is due to a slower increase of the hyperon content with density.

If the  $\sigma^*$  meson is not included and a repulsive hyperon-hyperon interaction is considered although a larger  $L$  gives rise to a larger strangeness content, the extra repulsion between hyperons due to the presence of the  $\phi$ -meson compensates for the extra hyperon fraction

and the effect of the symmetry energy is almost not seen on the central density of the maximum mass configuration. Using a harder EOS such as TM1-2 a larger hyperon fraction is obtained for a given density. Due to the extra hardness and the repulsive effect of the  $\phi$  meson, matter is less compressible and stars with larger strangeness content are more massive.

The identified uncertainties will certainly affect the appearance of other degrees of freedom, namely quark degrees of freedom, and we should expect a transition to a deconfined phase at lower densities for a harder hadronic EOS. The effect of the hyperon couplings and density dependence of the EOS on the metastability of hyperonic matter to the conversion to quark stars [32] should be investigated.

There is still lacking a lot of information about the nucleonic EOS at supra-saturation densities as well as on the hyperon interactions in nuclear matter that may allow that an unambiguous answer is given to the question whether the mass of the pulsar J1614-2230 could rule out exotic degrees of freedom from the interior of compact stars. We also conclude that some star properties are affected in a similar way by the density dependence of the symmetry energy and the hyperon content of the star. To disentangle these two effects it is essential to have a good knowledge of the EOS at supra-saturation densities. Low mass stars will probably involve only nucleonic degrees of freedom and will allow to study the density dependence of the symmetry energy effect alone. However, they will also only test densities not larger than  $2-3\rho_0$ .

## Acknowledgments

We would like to thank João da Providência for the reading of the manuscript and for many helpful and elucidating discussions. This work was partially supported by COMPETE/FEDER and FCT (Portugal) under the grant PTDC/FIS/113292/2009, and by COMPSTAR, an ESF Research Networking Programme.

- 
- [1] P. B. Demorest *et al*, *Nature* **467**, 1081 (2010).
  - [2] I. Vidaña, D. Logoteta, C. Providência, A. Polls, and I. Bombaci, *EPL* **94**, 11002 (2011).
  - [3] Simon Weissenborn, Debarati Chatterjee, Jürgen Schaffner-Bielich, *Nucl. Phys. A* **881**, 62 (2012).
  - [4] Simon Weissenborn, Debarati Chatterjee, Jürgen Schaffner-Bielich, *Phys. Rev. C* **85**, 065802 (2012)
  - [5] I. Bednarek, P. Haensel, J. L. Zdunik, M. Bejger, and R. Mańka *Astronomy & Astrophysics* **543**, A157 (2012)
  - [6] L. Bonanno and A. Sedrakian, *Astron. Astrophys.* **539**, A16 (2012).
  - [7] P. K. Panda, A. M. S. Santos, D. P. Menezes, and C. Providência, *Phys. Rev. C* **85**, 055802 (2012).
  - [8] M. Baldo, G. F. Burgio, and H-J Schulze, *Phys. Rev. C* **61**, 055801 (2000); I. Vidaña, A. Polls, A. Ramos, L. Engvik, and M. Hjorth-Jensen, *Phys. Rev. C* **62**, 035801 (2000); H.-J. Schulze, A. Polls, A. Ramos, and I. Vidaña, *Phys. Rev. C* **73**, 058801 (2006).
  - [9] S. Balberg and A. Gal, *Nucl. Phys. A* **625**, 435 (1997).
  - [10] B. D. Serot and J. D. Walecka, *Int. Jour. Mod. Phys. E* **6**, 515 (1997).
  - [11] N.K. Glendenning, *Astrophys.J.* 293, 470 (1985). DOI: 10.1086/163253; N. K. Glendenning and S. A. Moszkowski, *Phys. Rev. Lett.* **67**, 2414 (1991).
  - [12] R. Knorren, M. Prakash, and P. J. Ellis, *Phys. Rev. C* **52**, 3470 (1995)
  - [13] Jürgen Schaffner and Igor N. Mishustin, *Phys. Rev. C* **53**, 1416 (1996).

- [14] B. M. Waldhauser, J. A. Maruhn, H. Stocker, and W. Greiner, Phys. Rev. C **38**, 1003 (1988).
- [15] P. Danielewicz, R. Lacey, and W. G. Lynch, Science **298**, 1592 (2002).
- [16] Y. Sugahara and H. Toki, Nucl. Phys. **A579**, 557 (1994).
- [17] S. Typel and H. Wolter, Nucl. Phys. A **656**, 331 (1999).
- [18] Irina Sagert, Laura Tolos, Debarati Chatterjee, Jürgen Schaffner-Bielich, Christian Sturm, Phys. Rev. C **86**, 045802 (2012).
- [19] J. Aichelin and Che Ming Ko, Phys. Rev. Lett. **55**, 2661 (1985).
- [20] L. W. Chen, C. M. Ko, and B. A. Li, Phys. Rev. Lett. **94**, 032701 (2005).
- [21] C. J. Horowitz and J. Piekarewicz, Phys. Rev. C **64**, 062802 (2001).
- [22] R. Cavagnoli, D. P. Menezes, and C. Providência, Phys. Rev. C **84**, 065810 (2011).
- [23] J. Carriere, C. J. Horowitz, and J. Piekarewicz, Astrophys. J. **593**, 463 (2003).
- [24] B.G. Todd-Rutel and J. Piekarewicz, Phys. Rev. Lett. **95**, 122501 (2005).
- [25] A. Klimkiewicz *et al.*, Phys. Rev. C **76**, 051603(R) (2007); D. V. Shetty, S. J. Yennello, and G. A. Souliotis, Phys. Rev. C **76**, 024606 (2007); M. B. Tsang *et al.*, Phys. Rev. Lett. **102**, 122701 (2009); M. Centelles, X. Roca-Maza, X. Viñas, and M. Warda, Phys. Rev. Lett. **102**, 122502 (2009); M. Warda, X. Viñas, X. Roca-Maza, and M. Centelles, Phys. Rev. C **80**, 024316 (2009); Andrea Carbone, Gianluca Colò, Angela Bracco, Li-Gang Cao, Pier Francesco Bortignon, Franco Camera, and Oliver Wieland, Phys. Rev. C **81**, 041301 (2010).
- [26] A. Gal, Prog. Theor. Phys. Suppl., **186** 270 (2010); and references therein.
- [27] A. Gal and D. Millener, Phys. Lett. B **701**, 342 (2011).
- [28] C. Providência, R. Cavagnoli, D. P. Menezes, P. K. Panda and A. Rabhi, J. Phys: Conf. Seri. **413**, 012023 (2013).
- [29] J. R. Oppenheimer and G. M. Volkoff, Phys. Rev. **55**, 374 (1939); R. C. Tolman, Phys. Rev. **55**, 364 (1939).
- [30] G. Baym, C. Pethick, and P. Sutherland, Astrophys. J. **134**, 683 (1971)
- [31] D. J. Champion, *et al.*, Science **320**, 1309 (2008).
- [32] I. Bombaci, I. Parenti, and I. Vidaña, Astrophys. J. **614**, 314 (2004); I. Bombaci, D. Logoteta, C. Providência, and I. Vidaña, Astron. Astrophys. **528**, A71 (2011); D. Logoteta, I. Bombaci, C. Providência, and I. Vidaña, Phys. Rev. D **85**, 023003 (2012).